Correlation Between Local Hemodynamics and Lesion Distribution in a Novel Aortic Regurgitation Murine Model of Atherosclerosis

Yiemeng Hoi,[1] Yu-Qing Zhou,[2] Xiaoli Zhang,[2,3] R. Mark Henkelman,[2,3] and David A. Steinman[1]

[1]Biomedical Simulation Laboratory, Department of Mechanical & Industrial Engineering, University of Toronto, Toronto, ON, Canada; [2]Mouse Imaging Centre, The Hospital for Sick Children, Toronto, ON, Canada; and [3]Department of Medical Biophysics, University of Toronto, Toronto, ON, Canada

Associate Editor Joan Greve oversaw the review of this article.

Abstract—Following surgical induction of aortic valve regurgitation (AR), extensive atherosclerotic plaque development along the descending thoracic and abdominal aorta of $Ldlr^{-/-}$ mice has been reported, with distinct spatial distributions suggestive of a strong local hemodynamic influence. The objective of this study was to test, using image-based computational fluid dynamics (CFD), whether this is indeed the case. The lumen geometry was reconstructed from micro-CT scanning of a control $Ldlr^{-/-}$ mouse, and CFD simulations were carried out for both AR and control flow conditions derived from Doppler ultrasound measurements and literature data. Maps of time-averaged wall shear stress magnitude (TAWSS), oscillatory shear index (OSI) and relative residence time (RRT) were compared against the spatial distributions of plaque stained with oil red O, previously acquired in a group of AR and control mice. Maps of OSI and RRT were found to be consistent with plaque distributions in the AR mice and the absence of plaque in the control mice. TAWSS was uniformly lower under control vs. AR flow conditions, suggesting that levels (>100 dyn/cm^2) exceeded those required to alone induce a pro-atherogenic response. Simulations of a straightened CFD model confirmed the importance of anatomical curvature for explaining the spatial distribution of lesions in the AR mice. In summary, oscillatory and retrograde flow induced in the AR mice, without concomitant low shear, may exacerbate or accelerate lesion formation, but the distinct anatomical curvature of the mouse aorta is responsible for the spatial distribution of lesions.

Keywords—Computational fluid dynamics, Atherosclerosis, Plaque, Mouse models, Aorta, Oscillatory shear, Relative residence time, Wall shear stress.

Address correspondence to David A. Steinman, Biomedical Simulation Laboratory, Department of Mechanical & Industrial Engineering, University of Toronto, Toronto, ON, Canada. Electronic mail: steinman@mie.utoronto.ca

INTRODUCTION

Over the last decades, several genetically engineered mice have been successfully used to study the pathogenesis of atherosclerosis.[11,21] In a recent study that utilized low density lipoprotein receptor-deficient ($Ldlr^{-/-}$) mice, Zhou *et al.*[33] found that following the surgical induction of aortic valve regurgitation (AR), atherosclerotic plaques developed extensively along the descending thoracic aorta (DTAo) and abdominal aorta, which were naturally lesion free (Fig. 1a). Doppler ultrasound revealed that the aorta in the control mice faced a consistently antegrade flow except for the inner curvature of the aortic arch where a brief, early diastolic retrograde flow was detected and plaque was observed. In the AR mice, the whole aorta experienced an oscillatory flow pattern induced by the diastolic retrograde flow. Interestingly, the plaque found in the AR mice did not form evenly along the entire DTAo, but presented a distinct distribution which was seemingly relevant to the anatomical curvature of the aortic segment between the DTAo and proximal abdominal aorta, whereas such plaque distribution was absent in the corresponding locations in the control mice. Notably, the spatial patterns of plaque distribution in the AR mice were qualitatively consistent across the seven mice studied.[33] Although the AR-induced oscillatory, retrograde flow pattern turned the lesion resistant aortic region susceptible to plaque formation, it is unclear how the flow and natural curvatures of the DTAo affect the susceptibility of aortic regions to atherogenesis. As a step toward understanding the hemodynamic environment within which atherosclerosis develops in this murine model, the current study aimed to test whether the lesion distribution in the AR models is indeed associated with
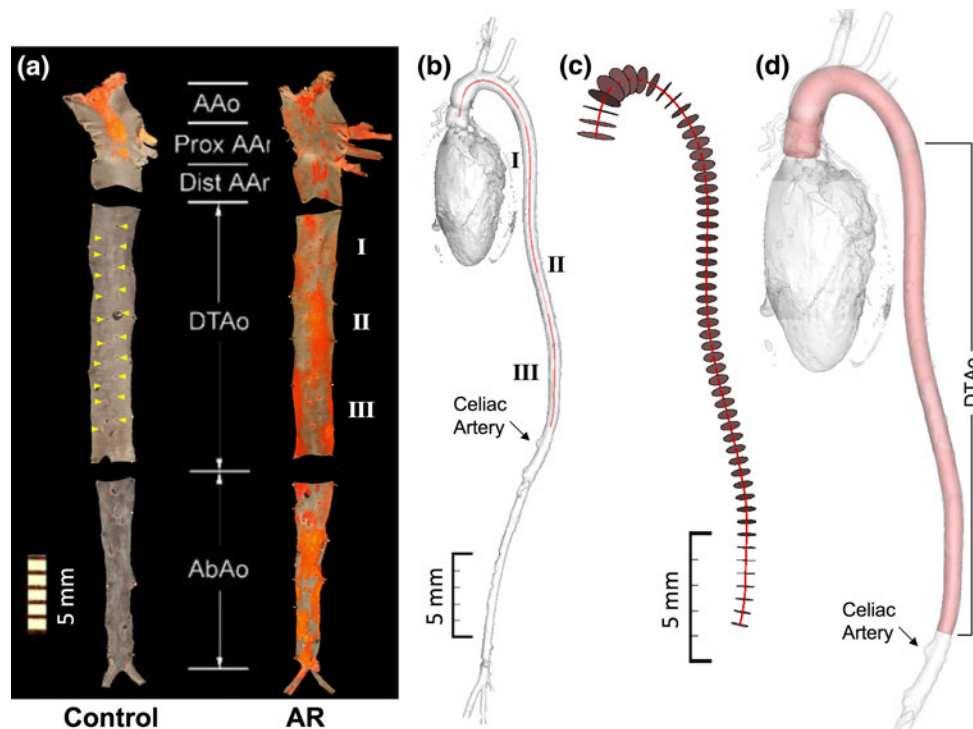
FIGURE 1. Oil red O stains and model construction. (a) En face topology of the stained lesions, showing (*left*) a control mouse free of plaque in the descending thoracic aorta (DTAo) and (*right*) AR mouse aorta stained with defined regions of plaque at the proximal (region I), middle (region II), and distal (region III) segments of DTAo. *Arrows* on the control staining point to the locations of the intercostal arteries. Adapted from Zhou *et al.*,[33] with permission. (b) Surface model extracted from the micro-CT scanning of a control mouse, also showing the automatically computed centerlines. (c) The centerline and the lumen radius were smoothed and subsequently lofted (showing every 15 slices along the centerline) to construct a surface model for image-based CFD analysis. (d) The computational geometry overlaid on the 3D surface model from micro-CT volume, showing minimal changes due to the lofting and smoothing operations of the model construction.

patterns of "disturbed" flow. (Hereafter, the quotes for this vague term are implied.)

MATERIALS AND METHODS

Mouse Imaging and 3D Geometry Construction

The present study focused on $Ldlr^{-/-}$ mice, as detailed by Zhou *et al.*[33] Briefly, AR was created by catheterization via the right common carotid artery at 14 weeks of age. In the control group, on $Ldlr^{-/-}$ mice of the same age and on the same cholesterol-enriched diet, sham catheterization was conducted without damaging the aortic valve. The experimental protocol was approved by the Animal Care Committee of the Hospital for Sick Children in Toronto, Ontario, Canada.

The aortic geometry was obtained from Microfil casting of a complete control mouse vasculature as described previously,[31] followed by partial dissection of the heart, aorta, and spine (to preserve anatomical shape). The specimen was subsequently scanned using micro-CT. The three-dimensional (3D) micro-CT data was digitally segmented using a level set method with a colliding front initialization as implemented in the open-source Vascular Modeling Toolkit (VMTK).[1] Due to the presence of bones, noise, and inhomogeneous cast fillings in the micro-CT images, the reconstructed surface, shown in Fig. 1b, had inadequate surface quality for direct image-based CFD analysis, especially towards the inferior region. To smooth the surface, we first used VMTK to automatically derive the centerline and its associated maximally inscribed sphere radii. Centerline coordinates and radii of the DTAo were then independently least-squares fit to third-order polynomial functions. Based on the smoothed centerline and lumen radius, we then lofted the circular cross-sections (Fig. 1c) with ICEM-CFD (ANSYS Inc., Canonsburg, PA) to construct the surface of the CFD model, which closely resembled the original aortic lumen (Fig. 1d).

As shown in Fig. 1d, the model used for CFD was truncated at the celiac artery, thereby including only the aortic arch and the DTAo. This was done to avoid the need for including the celiac, mesenteric, renal, and other inferior branches, the geometry and flow rates for which were difficult to resolve. The intercostal

arteries coming off the DTAo were excluded for similar reasons, and also because their fraction of DTAo flow is relatively small.[10] The three major upper extremity branches off the aortic arch were excluded from the computational geometry since they were not in the DTAo region of interest of this study, and the time-varying distributions of flow to these vessels were not known. Additionally, during the AR procedure, the right common carotid artery in the AR mice was ligated. The autoregulation process serves to redistribute and control flow to the other branches to maintain blood flow supply to the brain; however, it is unlikely that the blood flow supply to the brain is reversed during the instant where retrograde flow developed in the aorta of the AR mice. Without knowing the detailed instantaneous flow distributions in these major arteries off the aortic arch, we opted not to include them in the computational geometry to avoid unrealistic modeling results. On the other hand, the aortic arch segment was retained in order to act as a flow extension to ensure a more realistically skewed velocity profile entering the DTAo, not to predict the hemodynamics at the aortic arch itself.

It is worth noting that the measured mouse anatomy presents a tortuous descending aortic structure that bends three-dimensionally. Such a non-straight vascular structure will trigger complex flow patterns, which could be associated with spatial distribution of atherosclerotic lesions. To evaluate the influence of the actual aortic geometry on the disturbed flow exposure, we created for comparison an additional computational model by straightening the vessel beyond the aortic arch while maintaining the vessel size along the vessel length.

Flow Boundary Conditions

High frequency (30 MHz) pulsed Doppler measurements were made at 1 week post-surgery in both AR and sham control groups following previously described protocols.[32,33] Specifically, velocity spectra were acquired at the beginning of the DTAo distal to the left subclavian artery, a location referred to as L5 in Zhou *et al.*[33] Since these measurements were made under anesthesia, and anyway it is not straightforward to estimate flow rates from Doppler velocity traces due to uncertainties about velocity profile shape and Doppler artifacts, we elected to use them only to infer the *relative shapes* of the flow waveforms, to be scaled to *absolute* flow rates using data from the literature.

First, the maximum velocity of the Doppler spectrum was traced and three cardiac cycles were averaged to obtain the shapes of the systolic and diastolic phases of the control and AR waveforms (Fig. 2). Second, we scaled these to a heart rate of 435 bpm, obtained by
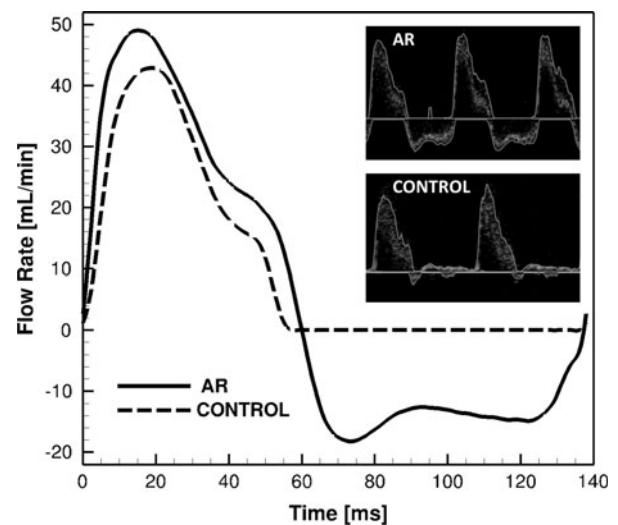

FIGURE 2. **Flowrate waveforms at the proximal descending aorta in the AR (*solid*) and control (*dashed*) cases, derived from Doppler ultrasound spectral graphs (*inset*) and literature data as described in the "Materials and Methods" section.**

averaging over a group of control and AR mice.[33] Third, we scaled the systolic phases of the AR and control waveforms so that their time velocity integrals (TVI) were 1.3:1, calculated from the average of the systolic TVI ratio (AR:control = 3.4:2.5) and cardiac output (CO) ratio (AR:control = 32.5:26.4) reported for the L5 segment by Zhao *et al.*[33] Fourth, the diastolic phase of the AR waveform was scaled to a TVI 1.8 times lower than its systolic phase, reflecting the 1.9:3.4 diastolic:systolic TVI ratio averaged over the greater and lesser curvatures at the L5 segment.[33]

Together the above steps provided the relative shapes of the AR and control flow waveforms. Then, assuming zero diastolic flow for the control case, we scaled the control waveform to a cycle-averaged flow rate of 16 mL/min, estimated by Feintuch *et al.*[7] for flow at the aortic root. The cycle-averaged flow rate for the AR waveform, being effectively fixed to the control waveform shape via the TVI ratios as described above, was 9.5 mL/min. Since our intention was to prescribe flow rates appropriate to the proximal DTAo—as noted above, the aortic arch was included only to ensure physiologically skewed velocity profiles entering the DTAo—the waveforms were finally rescaled by a factor of 0.64, accounting for the roughly 36% of flow expected to enter the great vessels off the arch[10] (which, as also noted above, were not included owing to the unknown instantaneous flow divisions for the AR case).

Numerical Simulation

The surface models were imported into ICEM-CFD and used to generate a finite element mesh of quadratic

tetrahedral elements. The final mesh contained approximately 400,000 quadratic elements (roughly equivalent to 3.2 million linear elements) with node spacing of 93 μm, found by mesh refinement studies to be more than adequate for resolving the wall shear stress patterns. The unsteady Navier–Stokes equations were solved using a previously validated in-house solver[6,19] with either control or AR flow waveforms as boundary conditions on the anatomical model. For the straightened model, only hemodynamics derived using the AR waveform were computed. A plug profile, scaled to the instantaneous flow rate, was imposed at the ascending aorta inlet and traction-free boundary conditions were imposed at the outlet. Rigid walls, a constant blood viscosity of 0.035 cm^2/s, and blood density of 1.06 g/cm^3 were assumed. The time-averaged Reynolds numbers, based on the 0.90 mm diameter of the proximal DTAo, were 41 and 69 for AR and control models, respectively. The Womersley number, also at the proximal DTAo, was 1.6 for both the AR and control models.

The CFD simulations were carried out using at least 4800 time steps per cardiac cycle, and at least three cycles were simulated to damp initial transients. For each model, we computed the time-averaged wall shear stress magnitude (TAWSS), the oscillatory shear index (OSI), and the relative residence time (RRT), which have been previously suggested as metrics of disturbed flow.[15] As defined by Himburg *et al.*,[9] RRT is inversely proportional to the product of TAWSS and $(1 - 2 \times \text{OSI})$, and should be normalized by a reference value, which we chose to be the RRT predicted for fully developed flow at the proximal DTAo of the AR model. TAWSS was not normalized and is reported in customary units of dyn/cm^2. OSI is an inherently dimensionless quantity, ranging in value from 0 to 0.5.

Hemodynamic Mapping

To directly compare the hemodynamic distributions with the lesions, we first isolated the DTAo of the computational model. For the *en face* preparations the region identified as DTAo in Fig. 1a was cut from the anterior surface between the diaphragm and first intercostal arteries. To mimic this, we first trimmed the computational model between these locations at planes normal to the centerline, as shown in Fig. 3a. This DTAo segment was then split automatically along an anterior line defined by the centerline parallel transport axes (Fig. 3b), which naturally follow the curve of the vessel.[1] This line was rotated about the centerline from its arbitrary reference orientation to an anterior position that approximately bisected the (posterior) intercostal branches. As shown in Fig. 3c, the objectively unfolded surface allows direct comparison of the
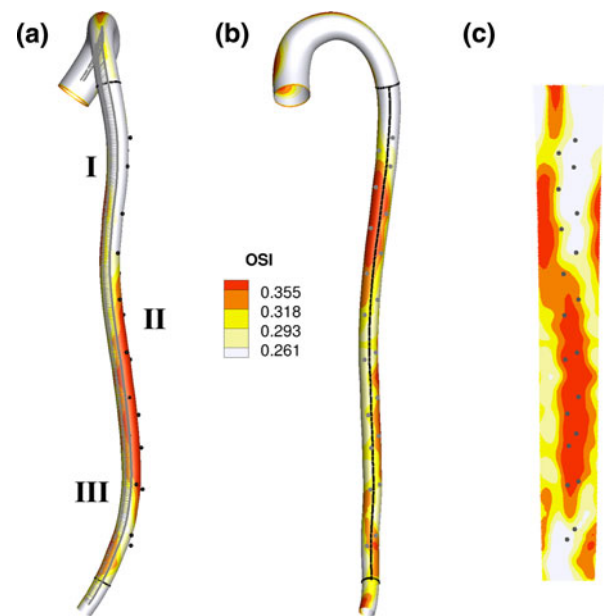

FIGURE 3. Process of mapping CFD results onto a plane, in this case OSI predicted under AR flow conditions. (a) Sagittal view of the 3D CFD model, showing the centerline and associated parallel transport vectors. Note the positions of the intercostals on the posterior (*right*) side, and the clipping planes near the *top* and *bottom*, defining the DTAo segment. Regions labeled I, II, and III are the same as those identified in Fig. 1. (b) Coronal view of the 3D CFD model, showing the anterior cutting line defined by the parallel transport vectors in panel A. Note how well this line, defined automatically, falls between the (posterior) intercostals, mimicking the protocol used to dissect the actual aortas as described by Zhou *et al.*[33] (c) The flattened OSI map for the DTAo segment, showing also the mapped locations of the intercostals pairs. Note how well these agree with the locations of the intercostal pairs seen in the *en face* stainings of Fig. 1a.

distribution of the hemodynamic quantities, and the positions of the intercostal branches agree well with those from the staining results (e.g., Fig. 1a).

RESULTS

Hemodynamics of AR vs. Control Mice

As shown in Fig. 4, patterns of disturbed flow for the AR model (panel b) demonstrated qualitative agreement with the consistent spatial distribution of plaques shown in panel a and also in Zhou *et al.*[33] Specifically, spiral-flow-induced circumferential variations in elevated OSI and RRT along the DTAo reflected the posterior and medial plaque distributions evident in regions II and III, respectively. The locations of elevated OSI and RRT in region I were also consistent with one case having plaques at the proximal DTAo. Circumferential variations in TAWSS broadly mirrored those of OSI and RRT; however, taper-induced increases in TAWSS along the DTAo
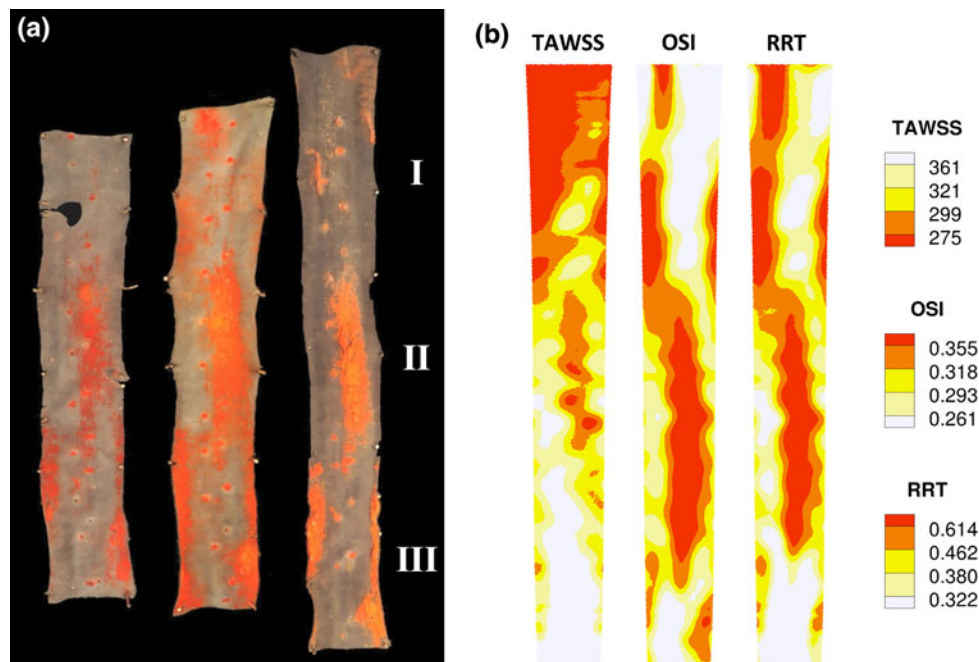
FIGURE 4. Comparison of plaque distribution and spatial distribution of TAWSS, OSI, and RRT for the AR case. (a) *En face* staining of three mice with severe AR, corresponding to the spectral Doppler waveform *inset* in Fig. 2. Note the consistent posterior staining of region II and medial staining of region III, whereas medial-posterior staining of region I is seen only for the middle case. (b) TAWSS, OSI, and RRT plotted at levels corresponding to quintiles of their respective distributions over the mapped surface, i.e., the 20th, 40th, 60th, and 80th percentile levels identified by the legends to the right. Note the scale is inverted for TAWSS to highlight regions of low shear (c.f., elevated OSI and RRT). For example, *red* (*dark*) highlights the 20% of mapped area exposed to the highest levels of OSI and RRT or the lowest levels of TAWSS.

were inconsistent with the predominance of plaques in regions II and III vs. region I.

Referring to Fig. 5, only the negligible levels of OSI under control flow conditions (<0.015 everywhere) were consistent with the absence of plaques in the control mice. As suggested by the contours delineating the regions of lowest TAWSS, circumferential variations in TAWSS under control flow conditions were similar to those under AR flow conditions, reflecting the geometry-induced spiral flow; however, TAWSS levels were roughly half of those for the control vs. AR model (e.g., 20th percentile of 137 vs. 275 dyn/cm^2), seemingly inconsistent with the *absence* of plaques in the former vs. the latter. RRT levels under control flow conditions were roughly 60% lower than those under AR flow conditions (e.g., 80th percentile of 0.375 vs. 0.614), consistent with the absence of plaques in the control mice except in region I, where RRT levels (~0.5) approached those in regions where plaques were evident in the AR mice.

Hemodynamics of Anatomical vs. Straight models

In contrast to the anatomical AR model, the straightened AR model (Fig. 6) exhibited different hemodynamics despite both models experiencing the same flow waveforms. The TAWSS in the straight

model increased along the vessel as it did for the anatomical model, but the absence of aortic curvature resulted in circumferentially uniform TAWSS distributions. Except for a spot of elevated OSI and RRT posterior at the proximal DTAo, the rest of the DTAo similarly displayed relatively uniform OSI and RRT distributions in the straight model. In other words, despite being exposed to the same retrograde AR flow as the anatomically realistic geometry, the straightened geometry did not produce a hemodynamic distribution consistent with the experimental spatial distribution of plaque in the AR mice.

DISCUSSION

Among those hemodynamic variables examined in the current study, OSI and RRT demonstrated qualitative agreement with the spatial distribution of plaques in the AR mice, whereas the distribution and levels of lowest TAWSS were inconsistent with the absence of lesions in the control mice. The correspondence of hemodynamics and plaques found only in the AR cases confirms that the flow waveform with significant retrograde component during diastole is an important factor contributing to the plaque development in the AR mice. Relative to the anatomical
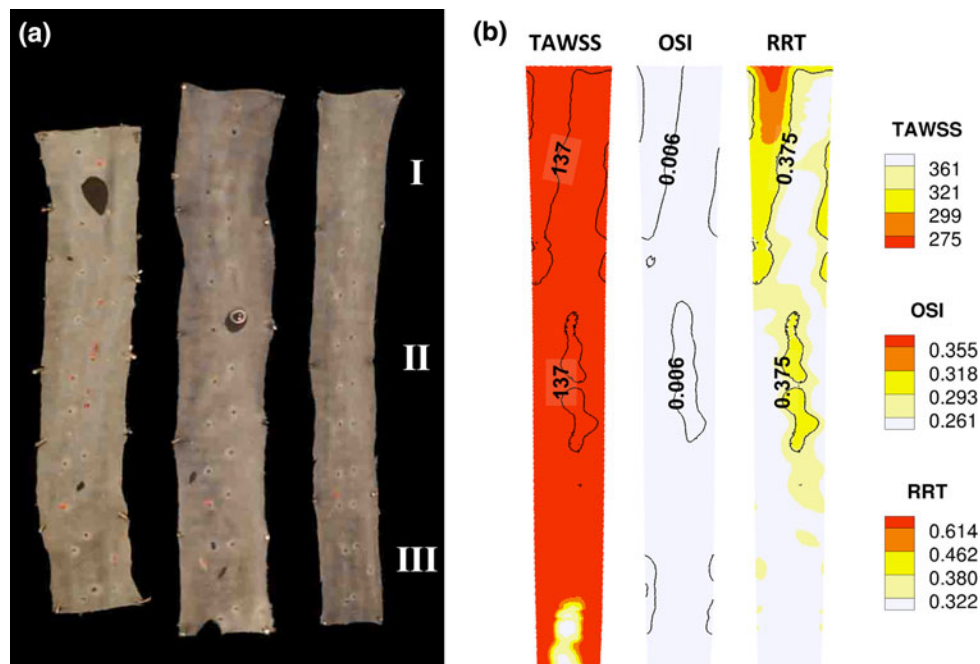
FIGURE 5. Comparison of plaque distribution and spatial distribution of TAWSS, OSI, and RRT for the control case. (a) En face staining of three control mice, demonstrating an absence of oil red O uptake except for small regions around the intercostals. (b) TAWSS, OSI, and RRT plotted at the same levels shown for Fig. 4 (i.e., quintiles of AR values). Contour lines, on the other hand, identify the regions and values corresponding to the upper quintile of the *control* OSI and RRT (for TAWSS, the lower quintile), in order to demonstrate the ''impression'' of the geometric influence despite the lower, non-atherogenic levels of disturbed flow. Note that the contour lines for TAWSS and RRT are identical, reflecting the fact that they are exactly equal to the inverse of one another when OSI ~ 0.
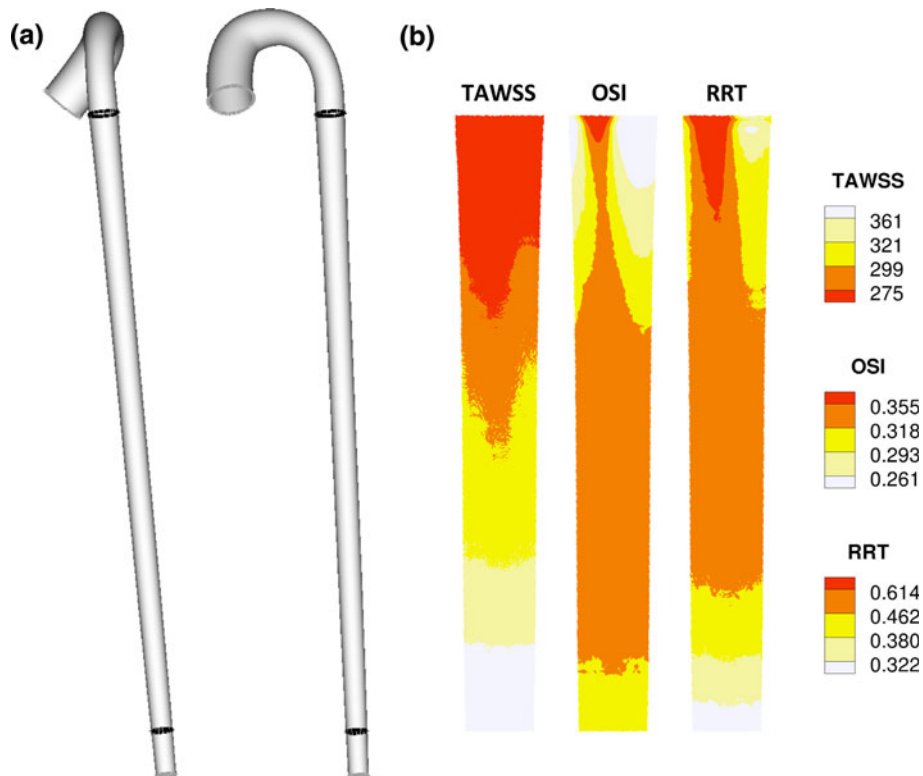

FIGURE 6. (a) Sagittal and coronal views of the straightened model. (b) Patterns of TAWSS, OSI, RRT predicted under AR flow conditions, plotted using the same contour levels as in Fig. 4.

model, the straight model produced uniform hemodynamics circumferentially, implying that important variations of hemodynamic parameters may be overlooked in simplified, straight vessel models of the mouse aorta.[10] Taken together, these data confirm that it is the *combination* of oscillatory retrograde flow and anatomical curvature, rather than either alone, that are responsible for the distinct patterns of plaque distribution in the AR model.

Disturbed flow has been suggested to play an important role in atherosclerosis; however, the term "disturbed" has not been well defined. Low and/or oscillatory shear are often used as markers of disturbed flow to infer the pathophysiology of atherosclerosis. TAWSS lower than some apparent physiological threshold has been suggested as pro-atherogenic in the human aorta.[3,18] In these regions, endothelial cells become dysfunctional, leading to compensatory responses that alter the normal homeostatic properties of the endothelium.[22] The upregulation of the proinflammatory mediators,[5,16,22] adhesion molecules,[23] and increased wall permeability[9] have been consistently reported in the lower TAWSS regions,[5,18] which supports the focal inflammatory process that likely underlies atherogenesis.[2,17,18,22,30] In the present study there appeared to be some concordance between the lowest levels of TAWSS in the AR model (150–300 dyn/cm^2) and locations of plaques in the AR mice at regions I and II (and possibly region III if we account for the ~20% reduction of flow along the DTAo due to the missing intercostal branches[10]). Presuming those levels of TAWSS to be atherogenic, it stands to reason that the control mice, which do not have plaques, should experience higher TAWSS. In fact the opposite is true: TAWSS levels in the control case were uniformly lower, a consequence of the definition of TAWSS as the average of WSS *magnitude* (i.e., the negligible diastolic WSS of the control case contributes less to the average than the absolute values of the appreciable negative diastolic WSS of the AR case). This suggests that low TAWSS *alone*, or at least the lowest levels observed here, are insufficient to explain lesions in the AR mice. Instead, any concordance between patterns of TAWSS and plaque distributions in the AR mice is merely a consequence of both being influenced by lumen geometry. Moreover, and consistent with other studies of mouse models,[4,8,23,26] the "low" TAWSS levels in the control model (on the order of 100 dyn/cm^2) exceed those thought to be pro-atherogenic in humans,[18] even if one accounts for allometric scaling.[27]

In atherosclerosis studies, high OSI is often accompanied by low TAWSS. The presence of low TAWSS, however, does not guarantee high OSI values.[13] This highlights the importance of oscillatory flow as a potentially atherogenic stimulus independent of low TAWSS. Regions exposed to high oscillatory, reversed flow are thought more susceptible to lesion formation.[14] The spatial distributions of OSI and plaques in the AR cases are consistent with this notion. When endothelial cells are exposed to oscillatory flow, they do not align with the flow or undergo cytoskeletal remodeling. In addition, they exhibit highly permeable intercellular gaps that facilitate intercellular transport of macromolecules,[9] leading to vascular dysfunction including intimal hyperplasia, platelet activation, inflammatory reaction, and reduced vasodilatation. Pro-inflammatory mediators, adhesion molecule expression, and fatty streak formation have been found to increase significantly in regions corresponding to oscillatory TAWSS.[5,23,28] Moreover, an increase in retrograde shear induces a dose-dependent attenuation of endothelial function in humans,[24] which underscores the possible detrimental effects of retrograde flow found in the AR mice.

Although the correspondence of the OSI map and plaque location in AR mice suggests that OSI is reliable in identifying pro-atherogenic hemodynamics, the mechanistic link between OSI and plaque development remains unclear. It has not been shown that the endothelial cells sense the OSI levels *per se*. Also, OSI is insensitive to TAWSS magnitudes. As pointed out by Himburg *et al.*,[9] these considerations suggest that OSI might better be employed in combination with other shear measures, namely in the form of a relative residence time, rather than as a stand-alone index of the flow. Remarkably, the RRT distribution of the AR model was also consistent with the spatial distribution of plaques in the AR mice. Prolonged residence time of atherogenic particles in the neighborhood of endothelium favors lipid exchange, recruitment of macrophages, and promotes the likelihood of plaque formation.[25,29,30] This mechanistic link suggests that elevated RRT, whether caused by low TAWSS *or* elevated OSI, may be useful as a *single* metric for identifying "disturbed flow" and its contribution to plaque formation.[15]

The spatial distribution of plaques suggests that contributing factors other than oscillatory retrograde flow potentially increase the likelihood of atherosclerotic lesions. Despite the relatively low average Reynolds numbers, the presence of anatomical curvature along the DTAo induces the formation of Dean-type spiral flow and consequent circumferentially varying distributions of shear in control and, to a greater degree, AR models. This is in marked contrast to the relatively uniform shear patterns demonstrated here in the straight model, and reported by Huo *et al.*[10] in their investigation of the hemodynamics in an idealized mouse aorta model composed of straight vessels. Taken together, our findings suggest that retrograde

flow may exacerbate or accelerate lesion formation in the AR model, but curved aortic geometry is responsible for the focal lesion distribution.

As with any model study, ours made a number of simplifying assumptions and approximations. We have assumed, for example, that flow patterns derived from this individual mouse aorta geometry are representative of those from other mice in the control and AR groups. Indeed there were interindividual variations in patterns of oil red O uptake that might be explained by a sensitivity of local hemodynamics to minor variations in aortic curvature; however, the broad patterns of plaque distribution, particularly in regions II and III, were consistent across mice, suggesting that the major curvatures of the DTAo, which are to some extent constrained by the anatomy, are likely consistent across these mice. The lumen geometry was also smoothed and pruned of branches, which served to ignore the potential influence of surface irregularities or non-circular lumen cross-sections and possible perturbations of the local flow patterns due to the great vessels off the arch and intercostal arteries running down the DTAo. Doppler ultrasound methodology was used to indirectly derive the CFD flow rate boundary conditions. Because of this novel mouse model, there is little information on the flow rates to other vascular territories, hindering us from inferring the flow in the branch vessels. Other imaging techniques, for instance using MR, ultrasound, or *in vivo* CT imaging technique with high spatial resolution could provide more accurate geometry and boundary conditions for CFD, particularly for the branch vessels. This study also made the customary assumption of a rigid wall. Closer to heart, the highly elastic mouse aorta experiences rapid deformation in addition to compliance-induced storage and release of flow along the DTAo, the former potentially introducing swirling flow into the ascending aorta,[12] and the latter potentially causing attenuation or dispersion of the flow waveform in the downstream vessels, as demonstrated in mice[33] as well as in humans.[20] Incorporating the aortic wall dynamics may be needed in future study, but it poses technical challenges in quantifying the spatial and temporal deformation in these small vessels. Nevertheless, despite these simplifications, there was remarkable agreement between the hemodynamic and plaque distributions, suggesting that the effects discussed above may be of second order to the distinct anatomic curvature of the mouse aorta.

CONCLUSION

Despite using a single, presumably representative mouse model, distributions of hemodynamic parameters OSI and RRT, but not TAWSS, qualitatively agreed with both the consistent spatial distribution of plaques found in AR mice and the absence of plaques in the control mice. Thus, oscillatory and retrograde flow induced in the AR mice, without concomitant low shear, may exacerbate or accelerate lesion formation. Our findings also highlight the importance of including anatomical curvature in CFD studies of murine hemodynamics, since these three-dimensional curvatures appear to drive the distinct spatial distribution of lesions seen in the AR mice. When carried out in a mouse-specific manner, it may be possible to link these hemodynamic metrics to the mechanisms of atherosclerosis in a more quantitative way.

REFERENCES

[1]Antiga, L., M. Piccinelli, L. Botti, B. Ene-Iordache, A. Remuzzi, and D. A. Steinman. An image-based modeling framework for patient-specific computational hemodynamics. *Med. Biol. Eng. Comput.* 46:1097–1112, 2008.

[2]Berk, B. C., J. I. Abe, W. Min, J. Surapisitchat, and C. Yan. Endothelial atheroprotective and anti-inflammatory mechanisms. *Ann. N. Y. Acad. Sci.* 947:93–109, 2001; (discussion 109–111).

[3]Caro, C. G. Discovery of the role of wall shear in atherosclerosis. *Arterioscler. Thromb. Vasc. Biol.* 29:158–161, 2009.

[4]Cheng, C., F. Helderman, D. Tempel, D. Segers, B. Hierck, R. Poelmann, A. van Tol, D. J. Duncker, D. Robbers-Visser, N. T. Ursem, R. van Haperen, J. J. Wentzel, F. Gijsen, A. F. van der Steen, R. de Crom, and R. Krams. Large variations in absolute wall shear stress levels within one species and between species. *Atherosclerosis* 195:225–235, 2007.

[5]Cheng, C., D. Tempel, R. van Haperen, A. van der Baan, F. Grosveld, M. J. Daemen, R. Krams, and R. de Crom. Atherosclerotic lesion size and vulnerability are determined by patterns of fluid shear stress. *Circulation* 113:2744–2753, 2006.

[6]Ethier, C. R., S. Prakash, D. A. Steinman, R. L. Leask, G. G. Couch, and M. Ojha. Steady flow separation patterns in a 45 degree junction. *J. Fluid Mech.* 411:1–38, 2000.

[7]Feintuch, A., P. Ruengsakulrach, A. Lin, J. Zhang, Y. Q. Zhou, J. Bishop, L. Davidson, D. Courtman, F. S. Foster, D. A. Steinman, R. M. Henkelman, and C. R. Ethier. Hemodynamics in the mouse aortic arch as assessed by MRI, ultrasound, and numerical modeling. *Am. J. Physiol. Heart Circ. Physiol.* 292:H884–H892, 2007.

[8]Greve, J. M., A. S. Les, B. T. Tang, M. T. Draney Blomme, N. M. Wilson, R. L. Dalman, N. J. Pelc, and C. A. Taylor. Allometric scaling of wall shear stress from mice to humans: quantification using cine phase-contrast MRI and computational fluid dynamics. *Am. J. Physiol. Heart Circ. Physiol.* 291:H1700–H1708, 2006.

[9]Himburg, H. A., D. M. Grzybowski, A. L. Hazel, J. A. LaMack, X. M. Li, and M. H. Friedman. Spatial comparison between wall shear stress measures and porcine arterial endothelial permeability. *Am. J. Physiol. Heart Circ. Physiol.* 286:H1916–H1922, 2004.

[10]Huo, Y., X. Guo, and G. S. Kassab. The flow field along the entire length of mouse aorta and primary branches. *Ann. Biomed. Eng.* 36:685–699, 2008.

[11]Ishibashi, S., M. S. Brown, J. L. Goldstein, R. D. Gerard, R. E. Hammer, and J. Herz. Hypercholesterolemia in low density lipoprotein receptor knockout mice and its reversal by adenovirus-mediated gene delivery. *J. Clin. Invest.* 92:883–893, 1993.

[12]Jin, S., J. Oshinski, and D. P. Giddens. Effects of wall motion and compliance on flow patterns in the ascending aorta. *J. Biomech. Eng.* 125:347–354, 2003.

[13]Knight, J., U. Olgac, S. C. Saur, D. Poulikakos, W. Marshall, Jr., P. C. Cattin, H. Alkadhi, and V. Kurtcuoglu. Choosing the optimal wall shear parameter for the prediction of plaque location-A patient-specific computational study in human right coronary arteries. *Atherosclerosis* 211:445–450, 2010.

[14]Ku, D. N., D. P. Giddens, C. K. Zarins, and S. Glagov. Pulsatile flow and atherosclerosis in the human carotid bifurcation. Positive correlation between plaque location and low oscillating shear stress. *Arteriosclerosis* 5:293–302, 1985.

[15]Lee, S. W., L. Antiga, and D. A. Steinman. Correlations among indicators of disturbed flow at the normal carotid bifurcation. *J. Biomech. Eng.* 131:061013, 2009.

[16]Libby, P. Inflammation in atherosclerosis. *Nature* 420:868–874, 2002.

[17]Libby, P., P. M. Ridker, and A. Maseri. Inflammation and atherosclerosis. *Circulation* 105:1135–1143, 2002.

[18]Malek, A. M., S. L. Alper, and S. Izumo. Hemodynamic shear stress and its role in atherosclerosis. *JAMA* 282:2035–2042, 1999.

[19]Minev, P. D., and C. R. Ethier. A characteristic/finite element algorithm for the 3-D Navier–Stokes equations using unstructured grids. *Comput. Methods Appl. Mech. Eng.* 178:39–50, 1998.

[20]Moore, J. E., Jr., S. E. Maier, D. N. Ku, and P. Boesiger. Hemodynamics in the abdominal aorta: a comparison of in vitro and in vivo measurements. *J. Appl. Physiol.* 76:1520–1527, 1994.

[21]Plump, A. S., J. D. Smith, T. Hayek, K. Aalto-Setala, A. Walsh, J. G. Verstuyft, E. M. Rubin, and J. L. Breslow. Severe hypercholesterolemia and atherosclerosis in apolipoprotein E-deficient mice created by homologous recombination in ES cells. *Cell* 71:343–353, 1992.

[22]Ross, R. Atherosclerosis—an inflammatory disease. *N. Engl. J. Med.* 340:115–126, 1999.

[23]Suo, J., D. E. Ferrara, D. Sorescu, R. E. Guldberg, W. R. Taylor, and D. P. Giddens. Hemodynamic shear stresses in mouse aortas: implications for atherogenesis. *Arterioscler. Thromb. Vasc. Biol.* 27:346–351, 2007.

[24]Thijssen, D. H., E. A. Dawson, T. M. Tinken, N. T. Cable, and D. J. Green. Retrograde flow and shear rate acutely impair endothelial function in humans. *Hypertension* 53:986–992, 2009.

[25]Tozer, E. C., and T. E. Carew. Residence time of low-density lipoprotein in the normal and atherosclerotic rabbit aorta. *Circ. Res.* 80:208–218, 1997.

[26]Trachet, B., A. Swillens, D. Van Loo, C. Casteleyn, A. De Paepe, B. Loeys, and P. Segers. The influence of aortic dimensions on calculated wall shear stress in the mouse aortic arch. *Comput. Methods Biomech. Biomed. Eng.* 12:491–499, 2009.

[27]Weinberg, P. D., and C. Ross Ethier. Twenty-fold difference in hemodynamic wall shear stress between murine and human aortas. *J. Biomech.* 40:1594–1598, 2007.

[28]Willett, N. J., R. C. Long, Jr., K. Maiellaro-Rafferty, R. L. Sutliff, R. Shafer, J. N. Oshinski, D. P. Giddens, R. E. Guldberg, and W. R. Taylor. An in vivo murine model of low-magnitude oscillatory wall shear stress to address the molecular mechanisms of mechanotransduction—brief report. *Arterioscler. Thromb. Vasc. Biol.* 30:2099–2102, 2010.

[29]Williams, K. J., and I. Tabas. The response-to-retention hypothesis of early atherogenesis. *Arterioscler. Thromb. Vasc. Biol.* 15:551–561, 1995.

[30]Williams, K. J., and I. Tabas. Atherosclerosis and inflammation. *Science* 297:521–522, 2002.

[31]Zhou, Y. Q., L. Davidson, R. M. Henkelman, B. J. Nieman, F. S. Foster, L. X. Yu, and X. J. Chen. Ultrasound-guided left-ventricular catheterization: a novel method of whole mouse perfusion for microimaging. *Lab Invest.* 84:385–389, 2004.

[32]Zhou, Y. Q., F. S. Foster, B. J. Nieman, L. Davidson, X. J. Chen, and R. M. Henkelman. Comprehensive transthoracic cardiac imaging in mice using ultrasound biomicroscopy with anatomical confirmation by magnetic resonance imaging. *Physiol. Genomics* 18:232–244, 2004.

[33]Zhou, Y. Q., S. N. Zhu, F. S. Foster, M. I. Cybulsky, and R. M. Henkelman. Aortic regurgitation dramatically alters the distribution of atherosclerotic lesions and enhances atherogenesis in mice. *Arterioscler. Thromb. Vasc. Biol.* 30:1181–1188, 2010.